Liquid Crystals
Publication details, including instructions for authors and subscription information:
http://www.informaworld.com/smpp/title~content=t713926090

Changing liquid crystal elastomer ordering with light - a route to opto-mechanically responsive materials

D. Corbett[a]; M. Warner[b]
[a] Department of Engineering Science, University of Oxford, Oxford, UK [b] Cavendish Laboratory, University of Cambridge, Cambridge, UK

First published on: 12 October 2009

To cite this Article Corbett, D. and Warner, M.(2009) 'Changing liquid crystal elastomer ordering with light - a route to opto-mechanically responsive materials', Liquid Crystals, 36: 10, 1263 — 1280, First published on: 12 October 2009 (iFirst)
To link to this Article: DOI: 10.1080/02678290903062994
URL: http://dx.doi.org/10.1080/02678290903062994

Liquid Crystals,
Vol. 36, Nos. 10–11, October–November 2009, 1263–1280

Taylor & Francis
Taylor & Francis Group

INVITED ARTICLE

Changing liquid crystal elastomer ordering with light – a route to opto-mechanically responsive materials

D. Corbett[a] and M. Warner[b]*

[a]*Department of Engineering Science, University of Oxford, Parks Road, Oxford OX1 3PJ, UK;* [b]*Cavendish Laboratory, University of Cambridge, 19 JJ Thomson Avenue, Cambridge CB3 0HE, UK*

(Received 8 April 2009; accepted 25 May 2009)

Long, flexible chains with rods and spacers give nematic polymer melts. Crosslinking yields highly extensible nematic elastomers. Molecular fluidity and orientational order are retained. Uniquely, these elastomers change shape drastically when orientational order is lost with temperature since chains lose their elongation. Reversible changes of 400% are easy to achieve. de Gennes envisaged this coupling between macroscopic strain and nematic (and other) liquid crystalline order.

Dye molecular rods are excited by photons into bent conformations. Bent rods depress orientational order and large thermal shape changes will be duplicated by light. Equally, rods may rotate away from the optical electric vector to avoid bending, thus also leading to mechanical strain. Mechanical recovery follows decay back to the molecular ground state. We sketch how these effects arise, explain how even polydomain networks deform under polarised and unpolarised light, and present new results on how nuclear magnetic resonance can reveal details of polydomain optical response. We explore non-linear absorption (photo-bleaching) leading to mechanical response where, by Beer's law, little light should theoretically penetrate.

In actuation, light penetrates quickly, is easy to deliver remotely, both excites and stimulates decay, and offers polarisation control over mechanics. Non-uniform director fields also control response. We illustrate novel photo-mechanical effects.

Keywords: photoisomerisation; nematic; elastomer; glass; actuation; non-linear; absorption

1. Introduction to nematic networks

In 1969 Pierre-Gilles de Gennes asked the question (*1*) 'What influence would liquid crystalline (LC) order have on the mechanics of a polymer network?'. He envisaged a nematic solvent elongating chains at the moment of crosslinking. The questions and the answers he proposed showed his usual great prescience: a nematic network would be able to reach an isotropic state on removal of the solvent, contracting along the director as orientational order was lost. He pictured chains elongated by nematic order and the mechanical state of the network reflecting this anisotropic distribution of molecular shapes. (He also considered cholesteric order and decided that topological imprinting (of twist) cannot be lost because of conflicting spatially dependent contractions, conclusions that are supported by explicit theory and experiment.) In 1975 he gave the first intimations (*2*) of intrinsically LC networks made by crosslinking liquid crystalline polymers, that, is polymers with incorporated rods that could order orientationally and thereby distort the backbone shape (see Figure 1).

The remarkable properties of liquid crystal elastomers follow from this connection that de Gennes identified. One requires, in addition to this molecular–macroscopic coupling, fluidity at the molecular scale so that conformations of the chains are mutually accessible. Then entropy continues to play a major role and the solid is rubbery, soft and capable of huge extensions. Order can be largely lost because the rods and chains can rearrange greatly. An additional vital freedom is also present – that of the director to rotate. We will see mechanical response, at constant nematic order, as a result of director rotation.

de Gennes was concerned with the loss of nematic order with temperature. It is very much a tribute to de Gennes that, in order to make sense of optical effects, we first review thermal effects in LC elastomers in some detail, exposing phenomena that were explicit and implicit in his early steps in the field. Our aim is then to extend these underlying thermal phenomena to the optical case where it is light that reduces nematic order, or rotates it, and we thus have dramatic opto-mechanical response.

Our review will be very de Gennesian. We concentrate on elastomers because there is a well-tested theoretical understanding and a molecular/director/order mobility that allows polymer and liquid crystal physics full applicability. More rigid (glassy) nematic networks

*Corresponding author. Email: mw141@cam.ac.uk

ISSN 0267-8292 print/ISSN 1366-5855 online

DOI: 10.1080/02678290903062994
http://www.informaworld.com

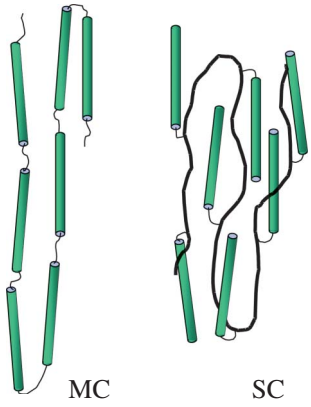

Figure 1. Main chain (MC) and side chain (SC) nematic polymers showing order of their rods and anisotropy of the backbone shape, as envisaged by de Gennes.

are also studied and are of considerable importance. We show their phenomena, but they still await a de Gennesian analysis.

First we give an experimental illustration of the effect we wish to describe: on heating and cooling a strip of nematic elastomer with its director along the strip, contraction and elongation, respectively, are observed, see for example the results of Tajbakhsh and Terentjev (*3*) and Figure 2.

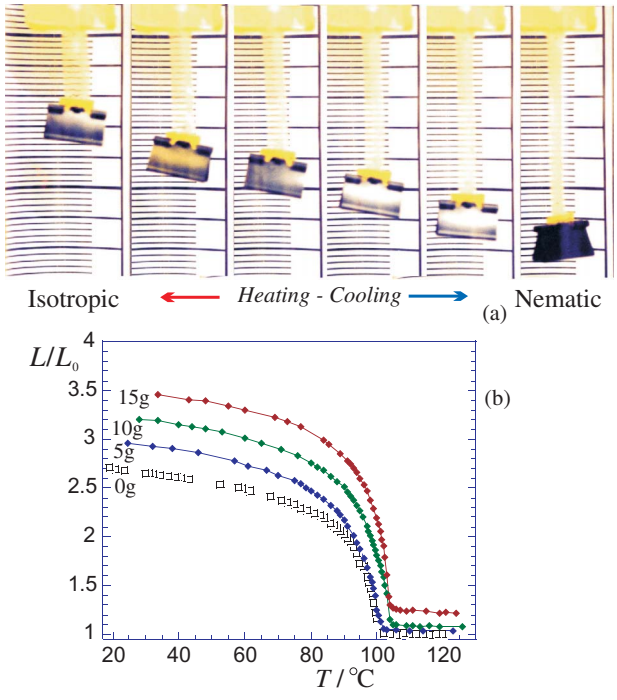

Figure 2. (a) Thermal elongation and contraction of nematic elastomer by 350%. (b) Relative shape change L/L_0 with temperature T while lifting various loads.

1.1 *Neo-classical elastomers*

Mechanical effects are very large, requiring a fully nonlinear picture of the energy and distortions. Linear theory, first developed by de Gennes (*4*), offers important guidance to the modes of distortion and how they couple to director rotation – the theory we sketch here reduces to the de Gennes limit. If the chains of Figure 1 are long enough, then in the melt their backbones take a Gaussian distribution of shapes. If ordered, their rods drive this distribution to be an anisotropic Gaussian. Since the backbones carry the elastic function of the network, it is those we henceforth concentrate on, see Figure 3.

The mean square end distances, the second moments, that characterise the Gaussian distribution of chain shapes are $\langle \underline{R}\,\underline{R}\rangle = \frac{1}{3}\underline{\underline{\ell}}L$ where L is the total arc length of a polymer and $\underline{\underline{\ell}}$ is the generalisation of the Flory step length to a tensor where the directions parallel and perpendicular to the director, $\underline{n}$, have different values, $\ell_\parallel$ and $\ell_\perp$, respectively. In specific and in coordinate-free forms, respectively, one has

$$\underline{\underline{\ell}} = \begin{pmatrix} \ell_\perp & 0 & 0 \\ 0 & \ell_\perp & 0 \\ 0 & 0 & \ell_\parallel \end{pmatrix} \equiv \ell_\perp \underline{\underline{\delta}} + [\ell_\parallel - \ell_\perp]\underline{n}\underline{n}\,. \qquad (1)$$

With the usual nematic order parameter $Q = \frac{3}{2}\langle\cos^2\theta\rangle - \frac{1}{2}$, a freely jointed polymer, with rods of length a, has the following simple form for $\underline{\underline{\ell}}$:

$$\underline{\underline{\ell}} = a\begin{pmatrix} 1-Q & 0 & 0 \\ 0 & 1-Q & 0 \\ 0 & 0 & 1+2Q \end{pmatrix}, \qquad (2)$$

whence

$$\ell_\parallel = a(1+2Q) \quad \text{and} \quad \ell_\perp = a(1-Q), \qquad (3)$$

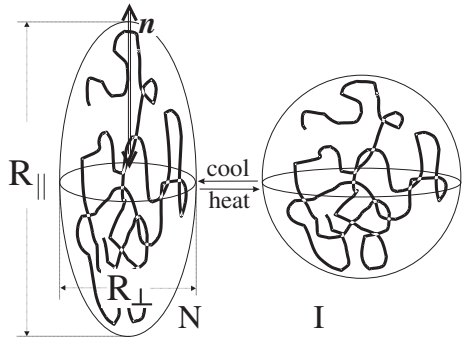

Figure 3. Typical chain backbones in the nematic and isotropic states, with their shape distribution being represented by the oblate and spherical shapes.

$$r = \frac{\ell_\parallel}{\ell_\perp} = \frac{1+2Q}{1-Q}, \tag{4}$$

the latter being the shape anisotropy, r, that largely determines the magnitude of the nematic elastomer response. The freely jointed chain model, although crude, seems to accurately model the properties of a wide range of MC and SC elastomers, see (*5*). The Gaussian distribution of chain conformations, $p(\underline{R})$, must be generalised for the anisotropic case:

$$p(\underline{R}) = \left[\left(\frac{3}{2\pi L}\right)^3 \frac{1}{\mathrm{Det}\left(\underline{\underline{\ell}}\right)}\right]^{\frac{1}{2}} \exp\left(-\frac{3}{2L} R_i \ell_{ij}^{-1} R_j\right). \tag{5}$$

Most polymer physics derives from the statistical weight of chains – here the probability, which is a reduced form of the partition function. We now use $p(\underline{R})$ to derive a slight modification of standard rubber elasticity to accommodate nematic order – a so-called 'neo-classical' free energy (*6*); see (*5*, *7*) for reviews. Figure 4 shows the current network with a current span $\underline{R}$ which derives from the initial span $\underline{R}_0$ established at crosslinking.

An unnecessary but convenient assumption is that spans change in geometric proportion to the body the network makes up, thus $\underline{R} = \underline{\underline{\lambda}} \cdot \underline{R}_0$ where $\underline{\underline{\lambda}}$ is the deformation gradient tensor. This tensor describes how a point initially at $\underline{X}^0$ in a body changes to another point $\underline{X}(\underline{X}^0)$ as $\underline{\underline{\lambda}} = \partial \underline{X}/\partial \underline{X}^0$. It also describes how the body as a whole changes shape; for instance, for a shape change the same at each point in the body and without shears, the current x dimension is given in terms of the initial as $X = \lambda_{xx} X^0$, and so on. Given that rubber is a soft solid (its bulk modulus is typically 10^4 times greater than its shear modulus), it deforms by changing shape at constant volume, thus one has $\mathrm{Det}\left(\underline{\underline{\lambda}}\right) = 1$.

Taking $-k_B T$ times the natural log of the statistical weight $p(\underline{R})$ gives the free energy of the span $\underline{R}$. Writing the current span vector $\underline{R}(\underline{R}_0)$ as a function of its initial span $\underline{R}_0$ one can average this free energy over the probability distribution $p(\underline{R}_0)$ of initial span vectors, which is given by

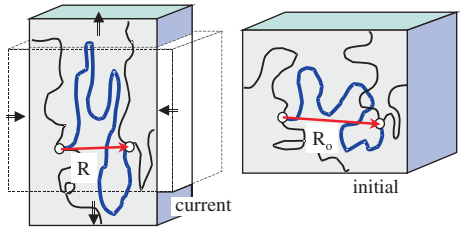

Figure 4. Current and initial states of the rubber and of a span in the network, that is, after and before macroscopic elongation.

$$p(\underline{R}_0) = \left[\left(\frac{3}{2\pi L}\right)^3 \frac{1}{\mathrm{Det}(\underline{\underline{\ell}}_o)}\right]^{\frac{1}{2}} \exp\left(\frac{-3}{2L} R_{0i} l_{oij}^{-1} R_{0j}\right). \tag{6}$$

The distribution $p(\underline{R}_0)$ is as in (5) but with the initial tensor $\underline{\underline{\ell}}_o$ instead. Averaging gives the free energy of the distorted distribution of spans. Multiplying by the number of spans per unit volume, n_x, and combining $n_x k_B T$ as μ, the shear modulus in the isotropic state, one has the free energy density of a nematic elastomer:

$$F = \frac{1}{2}\mu \mathrm{Tr}\left(\underline{\underline{\ell}}_o \cdot \underline{\underline{\lambda}}^{\mathrm{T}} \cdot \underline{\underline{\ell}}^{-1} \cdot \underline{\underline{\lambda}}\right) + \frac{1}{2}\mu \ln\left(\frac{\mathrm{Det}\left(\underline{\underline{\ell}}\right)}{\mathrm{Det}\left(\underline{\underline{\ell}}_o\right)}\right). \tag{7}$$

The first, Trace, term is what we shall use to derive the new dimensions of bodies on changing temperature and illumination and the energetic cost of deforming them. The second is needed only when considering the network energy derived from changing the nematic order, for instance on illumination. The expression is the equivalent of standard rubber elasticity, but where the initial and current shape distributions are recorded in the step length tensors.

1.1.1 *Spontaneous distortions*

Consider an initially isotropic elastomer, $\underline{\underline{\ell}}_o = a\underline{\underline{\delta}}$. In its current, relaxed, monodomain nematic state, the chains have a natural shape described by the tensor $\underline{\underline{\ell}}$. No stresses or constraints have been applied to it and thus any $\underline{\underline{\lambda}}$ is a *spontaneous* distortion, $\underline{\underline{\lambda}}_m$. From the symmetry of the phase that has developed on cooling, the distortion must be uniaxial and directed along $\underline{n}$. It must also be volume preserving. With a z-director, that is $\underline{n} = \underline{z}$, the deformation tensor $\underline{\underline{\lambda}}$ has its principal extension element λ along $\underline{z}$, whence the whole matrix $\underline{\underline{\lambda}}$ is

$$\underline{\underline{\lambda}} = \begin{pmatrix} 1/\sqrt{\lambda} & 0 & 0 \\ 0 & 1/\sqrt{\lambda} & 0 \\ 0 & 0 & \lambda \end{pmatrix} \equiv \underline{\underline{\lambda}}^{\mathrm{T}}. \tag{8}$$

The inverse step length tensor $\underline{\underline{\ell}}^{-1}$ in the same system of coordinate axes is

$$\underline{\underline{\ell}}^{-1} = \begin{pmatrix} 1/\ell_\perp & 0 & 0 \\ 0 & 1/\ell_\perp & 0 \\ 0 & 0 & 1/\ell_\parallel \end{pmatrix}. \tag{9}$$

Multiplying the four diagonal matrices $[(a\underline{\underline{\delta}}) \cdot \underline{\underline{\lambda}}^{\mathrm{T}} \cdot \underline{\underline{\ell}}^{-1} \cdot \underline{\underline{\lambda}}]$ gives

$$\mathrm{Tr}\begin{pmatrix} a/(\lambda\ell_\perp) & 0 & 0 \\ 0 & a/(\lambda\ell_\perp) & 0 \\ 0 & 0 & a\lambda^2/\ell_\parallel \end{pmatrix},$$

taking the trace results in

$$F = \frac{1}{2}\mu\left(\lambda^2\frac{a}{\ell_\parallel} + \frac{2}{\lambda}\frac{a}{\ell_\perp}\right). \tag{10}$$

Unloaded, the system adopts a spontaneous extension λ minimising the elastic free energy density (10). Taking $\partial F/\partial\lambda = 0$, we immediately conclude that on cooling there must be a spontaneous uniaxial elongation λ_m of (*8*, *9*)

$$\lambda_m = \left(\ell_\parallel/\ell_\perp\right)^{1/3} = r^{1/3}. \tag{11}$$

This is the spectacular length change we have seen, for instance, in Figure 2. It depends only on the anisotropy of the shape distribution, r. Confirmation of this theoretical picture had to await methods of fabricating monodomains that are due to Finkelmann (*10*). Part of our aim is to generalise this change to optical systems. We shall find that monodomains are no longer essential. Polydomain photo-elastomers react to light, indeed their mechanics can be controlled via the optical polarisation.

1.2 Soft elasticity

When strains are imposed externally on nematic elastomers, it turns out there is a low cost route for them to deform – by rotating the director at constant magnitude of nematic order. The constancy of order means no nematic energy cost is incurred. Rotation of the director means that the naturally elongated direction in the network can be aligned towards the direction that is being extended. Distortion of the distribution of chains can be at least partially avoided and the usual rubber elastic penalty is reduced. We shall be concerned with the optical response of complex systems such as polydomains, and we thus first review the routes to softer deformation that are found in non-optical nematic elastomers.

Consider the deformation gradient represented by the following expression, obscure as it may appear at first glance (*11*):

$$\underline{\underline{\lambda}} = \underline{\underline{\ell}}^{1/2} \cdot \underline{\underline{W}}_\alpha \cdot \underline{\underline{\ell}}_o^{-1/2}, \tag{12}$$

where $\underline{\underline{W}}_\alpha$ is an arbitrary rotation by an angle α. The current and initial states now have the same order Q and differ only in their directors $\underline{n}$ and $\underline{n}_o$. Considering the rotations connecting $\underline{n}$ and $\underline{n}_o$ and those associated with $\underline{\underline{W}}_\alpha$, this $\underline{\underline{\lambda}}$ represents a large number of potential distortions. If we insert such a deformation into the Trace formula, as well as its transpose $\underline{\underline{\lambda}}^T$, equivalent to $\underline{\underline{\ell}}_o^{-1/2} \cdot \underline{\underline{W}}_\alpha^T \cdot \underline{\underline{\ell}}^{1/2}$ since the $\underline{\underline{\ell}}$ are symmetric, we obtain

$$F_{el} = \frac{1}{2}\mu\mathrm{Tr}\Big(\underline{\underline{\ell}}_o \cdot \underline{\underline{\ell}}_o^{-1/2} \cdot \underline{\underline{W}}_\alpha^T \cdot \underbrace{\underline{\underline{\ell}}^{1/2} \cdot \underline{\underline{\ell}}^{-1} \cdot \underline{\underline{\ell}}^{1/2}}_{\underline{\underline{\delta}}} \cdot \underline{\underline{W}}_\alpha \cdot \underline{\underline{\ell}}_o^{-1/2}\Big) \equiv \frac{1}{2}\mu\mathrm{Tr}\left(\underline{\underline{\delta}}\right) = \frac{3}{2}\mu. \tag{13}$$

The middle section $\underline{\underline{\ell}}^{1/2} \cdot \underline{\underline{\ell}}^{-1} \cdot \underline{\underline{\ell}}^{1/2}$ gives the unit matrix $\underline{\underline{\delta}}$, by definition. The rotation matrix $\underline{\underline{W}}_\alpha$ then meets its transpose to also give unity: $\underline{\underline{W}}_\alpha^T \cdot \underline{\underline{W}}_\alpha = \underline{\underline{\delta}}$. Likewise disposing of the $\underline{\underline{\ell}}_o$ terms, one obtains the final value $F_{el} = \frac{3}{2}\mu$. This is identical to the free energy of an undistorted network. The non-trivial set of distortions $\underline{\underline{\lambda}}$ of the form Equation (12) has not raised the energy of the nematic elastomer! Figure 5 explains the principle.

Large strain and rotation experiments confirm this picture by following stress and director in response to an elongation applied perpendicular to the original director. The director rotates in response to present a longer dimension of the network to the strain direction (see Figure 6).

Rotation starts and ends in a singular fashion (*13*) as required by the soft deformation formula above. The characteristic forms shared by all samples collapses on to a master curve when appropriately reduced.

Stress is accordingly reduced, at least until director rotation is complete; see Figure 7.

One sees that stresses are reduced by orders of magnitude when director rotation is involved. In practice a responding elastomer will always suffer director rotation if it is possible, even at the cost of forming microstructures and textures of varying director

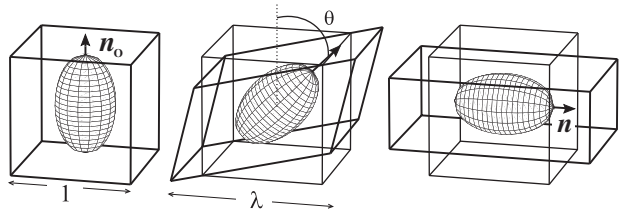

Figure 5. Application of an elongation λ perpendicular to the initial director induces the distribution of chains to rotate. Along with shears, the elongation is achieved simply by rearrangement rather than distortion. Soft response ceases on rotation by 90° where the long axis of the distribution is already aligned with the elongation.

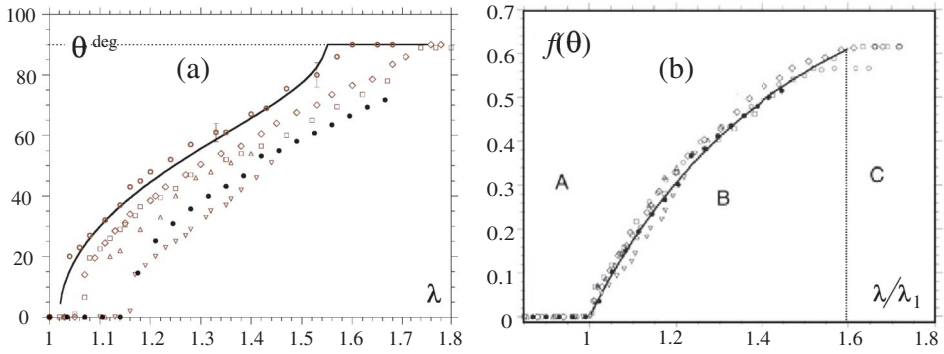

Figure 6. (a) Director rotation in response to an elongation imposed perpendicular to the director (*12*). (b) Collapse of rotation data on to a master curve arising from (12) against elongation reduced by the semi-soft threshold (*13*).

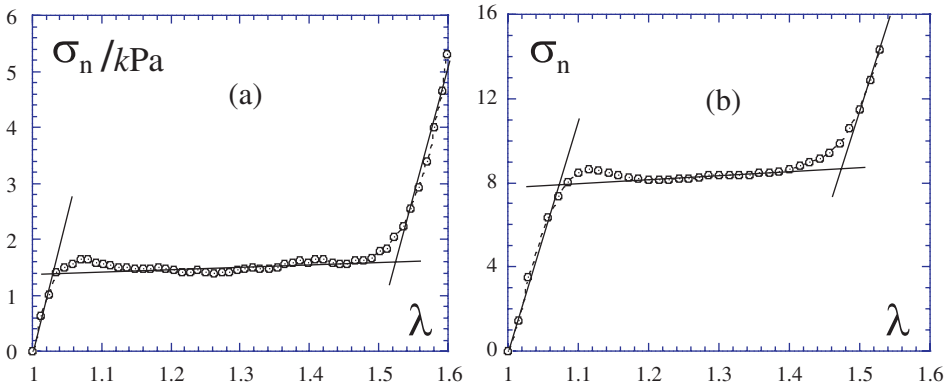

Figure 7. Stress in response to an elongation imposed perpendicular to the director (a) (*14*) and (b) Terentjev *et al.* (*5*).

rotation so that boundary constraints can still be respected.

Actually there is a threshold deformation before director rotation starts and the stress increases as in a conventional elastomer until this point. The threshold is due to non-ideality and such elasticity is known as semi-soft. This is one reason why small strain rheology (*15*) (with strains $10^3 - -10^4$ times smaller than here) is doomed to failure in investigating this aspect of nematic elastomer response. See (*16*) for conditions when and when not small strain rheology can see non-trivial nematic elastomer response. We shall find that director rotation can be important in facilitating mechanical response to light, particularly in polydomain nematic elastomers.

Freedom to rotate the director, and rubbery energy scales (with therefore constancy of volume when deforming) are two attributes important to nematic elastomer response which are not shared by nematic glasses. Such networks are more tightly cross-linked, have higher moduli, deform with volume change and suffer little or no director rotation. They can also have very subtle and rich thermal, optical and solvent response. Their optical study has been pioneered by Broer *et al.* (*17*, *18*), Ikeda *et al.* (*19*) and Tabiryan *et al.* (*20*). The principles on which they act differ greatly from elastomers. We shall illustrate later several important new phenomena they exhibit.

2. Photo-isomerisation in nematic networks

Some dye molecules, when they absorb a photon, suffer photoisomerisation, that is a change of molecular shape from their linear *trans* ground state to a bent *cis* excited state. Most notable is azo benzene and its derivatives which are shown in Figure 8 in two of the contexts we shall meet them – as crosslinkers in a nematic network or rods attached to the network's chains.

Alternatively, dyes can be guests dissolved in their rod-like host and still exercise influence over it. Photounits can form the core of a rod-like molecule that is spatially extended. Bend at the core can thereby cause profound molecular shape change. In any of these three guises, dye units when in a liquid crystalline

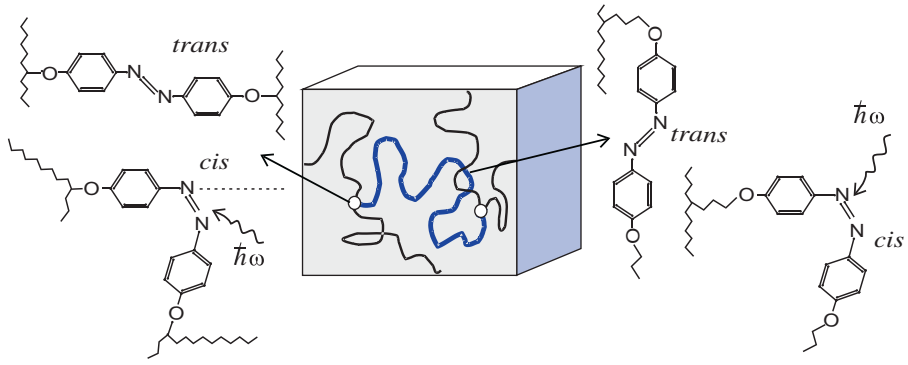

Figure 8. Azo-derivative dye molecules as active species in a nematic network; left as crosslinkers, right as pendant rods.

host can lower or remove the nematic order (*21*, *22*); see Figure 9. Other dyes absorb light in the green and orange rather than the ultraviolet (UV) as in this figure. At this stage we ignore attenuation of the optical beam as it passes through an elastomer, concentrating on uniform response.

The influence of photo-rods upon networks was first investigated in a sequence of papers by Eisenbach (*23–26*), who included photo-rods within an isotropic crosslinked polymer network. Initially the film was loaded with a weight W and allowed to elongate to its new equilibrium length. The sample was then subjected to the following illumination cycle: (i) illumination at $\lambda_1 = 365$ nm, which excites the *trans* $\rightarrow$ *cis* reaction; (ii) illumination at $\lambda_2 = 436$ nm, which excites the *cis* $\rightarrow$ *trans* reaction. During the first stage of the cycle the sample contracts as *cis* molecules are generated, while during the second stage the sample re-expands towards its initial state. The process is repeatable over many cycle. The generation of *cis* molecules reduces the Flory step length of the sample which increases the effective shear modulus of the material and thus lowers the strain required to accommodate the external weight W. Pre-strain is necessary for this kind of actuation.

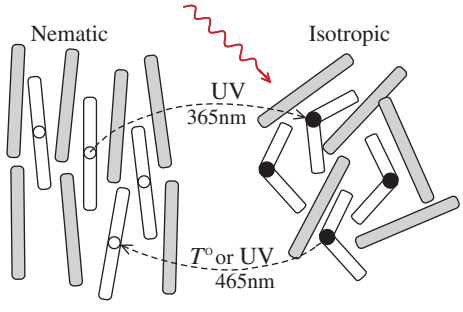

Figure 9. Dye guest molecules bend and disrupt the nematic order of their hosts. For azo dyes UV light is required. Back reaction is by thermal decay or stimulated decay by light of longer wavelength.

While remarkable, the effect noticed by Eisenbach was small, at most -0.25% strain. One can get much larger effects if the photo-rods can bend in a nematic network. As in dye–LC mixtures, the bent *cis* state does not contribute to nematic order nearly so well as the rod-like *trans* state. The generation of *cis* molecules thus lowers the order parameter Q within the network and produces a photo-mechanical response analogous to the thermo-mechanical response of Section 1.1.1 explained above. Finkelmann *et al.* (*27*) investigated the effects of incorporating azo chromophores within a monodomain nematic elastomer. They first measured the thermal deformations of their sample; see Figure 10(b). Following this they took a sample at several initial temperatures and illuminated with light of an appropriate colour to generate *cis* molecules; see Figure 10(a). The sample initially at 40°C undergoes a 22% contraction upon illumination, which can be seen to be nearly the full thermal contraction for a sample starting at this temperature. Conversely samples with lower starting temperatures undergo smaller photo-contractions – for samples further from the nematic–isotropic transition temperature, the optical disruption of the order parameter is insufficient to reach the isotropic phase. Later work has followed this strategy, taking slightly different nematic polymer architecture, see for instance (*28*).

In an early experiment, Cviklinski *et al.* (*29*) simultaneously measured the stress and the optical birefringence of a clamped monodomain nematic elastomer film with azo groups attached as pendants to the network (side-chain). Clamping the sample removes the possibility of strain and, since illumination leads to a contraction of the natural length of the sample, a stress develops. As shown in Figure 11, the birefringence, and thus the nematic order Q, follows the stress precisely in time, suggesting that it is ordering rather

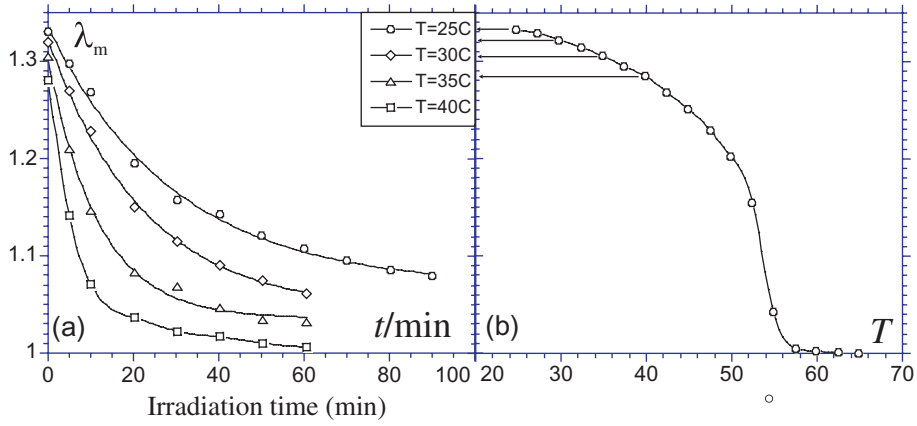

Figure 10. (a) Contraction along the director as a function of illumination time for various initial temperatures. (b) Contraction along the director as a function of temperature.

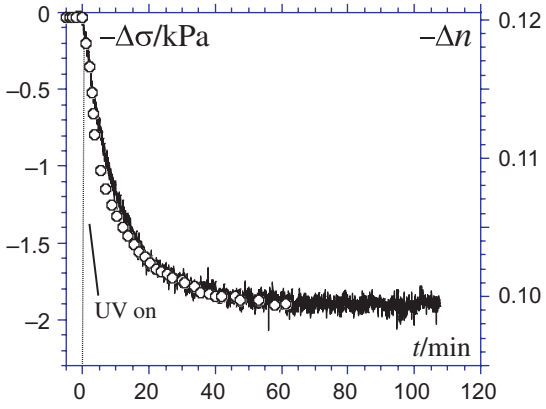

Figure 11. Build up of stress in a clamped, illuminated photo-elastomer, with the simultaneous measurement of nematic order reduction (*29*).

than temperature or illumination *per se* that drives mechanical response.

Indeed, taking the view that $Q(T)$ or $Q(I)$ drives $\lambda_m(Q)$, then one can map the thermal and optical responses on to each other. The solid lines in Figure 10(a) are calculated optical responses based on the mechanical response in Figure 10(b).

The temperature scale characteristic of a UV photon is roughly 10^4 K; one might thus imagine that the *trans* → *cis* → *trans* cycle causes significant heating of the network. Are the observed mechanical effects a consequence of this heating from absorption rather than a reduction in orientational order due to photo-isomerisation? Almost certainly both mechanisms can be important. However, many experiments in nematic elastomers and other nematic solids prove that optical effects can dominate, as we now see.

In the Finkelmann experiments, it was possible to return an illuminated sample most of the way back to its initial configuration by stimulating the *cis* → *trans* isomerisation optically with visible light. Characteristic temperatures of visible photons are still very high. If heating as a result of absorption was the dominant mechanism for generating a mechanical response, one would not expect the sample to return towards its original state. It is strongly suggested that there is an increase in orientational order as *trans* molecules are generated.

More conclusively, Harvey *et al.* (*30*) clamped a polydomain photo-elastomer and illuminated it with polarised light. Polydomain elastomers are particularly appealing since they are much easier to produce than nematic monodomains. For a given light intensity, the contractile force generated depended on $\cos^2\theta$ where θ was the angle between the long (clamped) dimension of the sample and the plane of polarisation of light. This experiment is remarkable in that a response in a polydomain system is achieved at all – thermally there can be no response since all domains want to contract, but in conflicting directions. Optically generated heat would diffuse quickly between the small domains and no thermal response would ensue. Clearly the effect is optical and moreover it is determined in direction by the polarisation – domains aligned closer to the optical electric field E are preferentially contracted. This effect was predicted theoretically in elastomers (*31*) and is the subject of Section 3.1. The ability to target the response using the polarisation direction of light is also a major advantage over thermal actuation.

Yu and Ikeda (*19*) produced thin films of a polydomain glassy network containing a high concentration of azo choromophores in the form of a crosslinker. Because of high crosslinking density, the materials are of high modulus and suffer smaller opto-mechanical responses. However, they bend substantially due to absorption giving a different light intensity with depth – a phenomenon we explore in

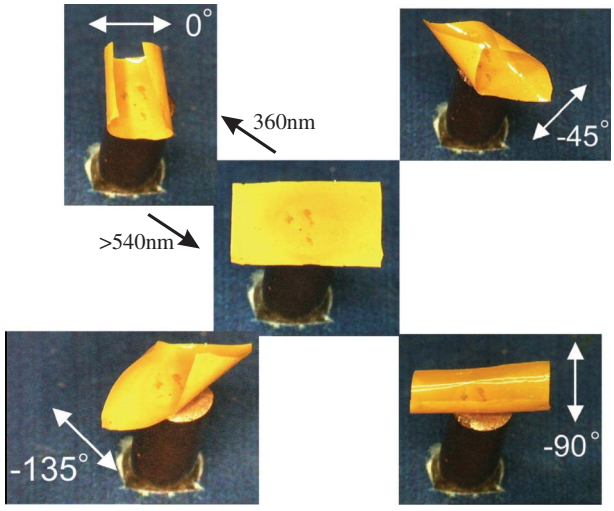

Figure 12. Development of curling along the direction of polarisation of incident light of wavelength 360 nm, followed by optically stimulated (visible > 540 nm) uncurling for thin glassy polydomain films (*32*).

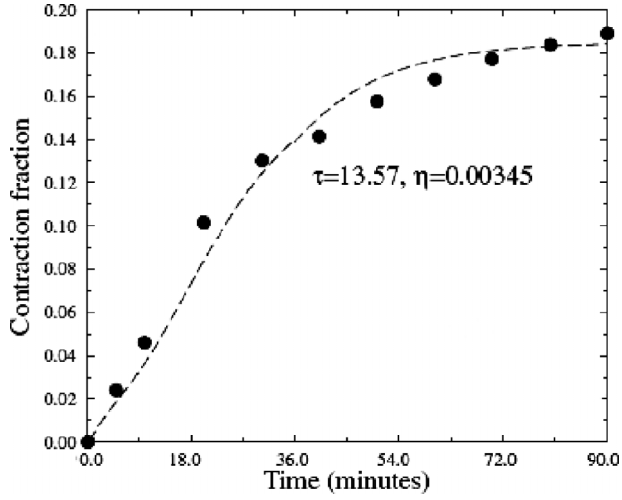

Figure 13. Theoretical fitting (dashed curve) of the contraction fraction versus time for the elastomer at $T = 298$ K, symbols are experimental data. Adapted from (*27*).

Section 4. Upon illumination with linearly polarised light, Yu and Ikeda's samples curled along the direction of polarisation. Uncurling could be achieved optically by irradiating with visible light; see the sequence in Figure 12.

Again, the actuation of a polydomain sample clearly indicates that the driving mechanism for the mechanical response is the change in orientational order as a result of photo-isomerisation. Such polarisation control has also been demonstrated in bending by White *et al.* (*33*) in both mono and polydomain glassy networks.

3. Theoretical description of nematic photo-elastomer response

In order to model the mechanical response of azo-containing elastomers it is essential to describe the population dynamics of the *trans* → *cis* process. In (*27*) simple population dynamics were assumed in which the *trans* molecules were excited into the *cis* state with rate ΓE^2 where E is the magnitude of the electric field. Simple thermal decay with a characteristic time τ was assumed for the *cis* configuration. Denoting the fraction of *trans* nematogens by n_t and that of *cis* by $n_c = 1 - n_t$ their dynamics are thus:

$$\frac{\partial n_t}{\partial t} = -\Gamma E^2 n_t + \frac{n_c}{\tau}, \qquad (14)$$

integration of which gives the time dependence of n_t. Finkelmann *et al.* (*27*) then go on to assume that the change in *trans* fraction reduces the strength of the nematic interactions, which is equivalent to increasing the operating temperature of the elastomer; they assume a form $T(t) = T_0(1 - n_t)^{-\epsilon}$ where T_0 is the initial temperature of the elastomer and ϵ is a parameter to be determined by fitting. This form for the temperature variation then allows a direct mapping between the optical and thermal responses of the elastomer where the parameters Γ, τ and ϵ are to be determined by the fit. Finkelmann *et al.* performed this fitting and, as shown in Figure 13, obtained an excellent fit.

The simple population dynamics proposed above, however, lacks a direct coupling between the order parameter Q and the rate of production of *cis* molecules. This is only acceptable if one is using diffuse illumination in which light comes from all directions. If polarised light is used, the magnitude of the order parameter is important (*31*, *34*). Consider a *trans* molecule with its long axis along $\underline{u}$; see Figure 14. The rate of isomerisation for such a molecule is $\Gamma(\underline{E}.\underline{u})^2$, that is, it is proportional to the intensity along the rod and to a cross section Γ. Thus the total

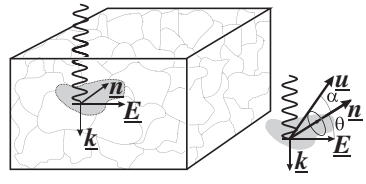

Figure 14. A thin film of polydomain nematic elastomer is illuminated by polarised light. A single domain with current director $\underline{n}$ is shown making angle θ with the optical field $\underline{E}$. Angles, α, of individual nematogens of axis $\underline{u}$, with respect to the director of the domain are also shown.

rate of isomerisation is given by $\Gamma\langle(\underline{E}.\underline{u})^2\rangle n_t$ where the average $\langle\cdots\rangle$ is taken over all orientations of the *trans* nematogens. The modified dynamics thus become

$$\frac{\partial n_t}{\partial t} = -\Gamma\langle(\underline{E}.\underline{u})^2\rangle n_t + \frac{(1-n_t)}{\tau}. \qquad (15)$$

Assuming linearly polarised light, the average rate of isomerisation is given by $\langle(\underline{E}.\underline{u})^2\rangle = E^2[Q(\cos^2\theta - 1/3) + 1/3]$ where θ is the angle the current director $\underline{n}$ makes with $\underline{E}$. The steady state *cis* fraction $\bar{n}_c = 1 - \bar{n}_t$ for a domain with director $\underline{n}$ is thus

$$\bar{n}_c = \frac{\Gamma\tau E^2\left[Q(3\cos^2\theta - 1) + 1\right]}{3 + \Gamma\tau E^2[Q(3\cos^2\theta - 1) + 1]}, \qquad (16)$$

where the combination $\Gamma\tau = 1/I_c$ can be interpreted as the reciprocal of the characteristic intensity I_c, which is a material constant.

Henceforth we reduce intensities $I = E^2$ by I_c to give $\tilde{I} = I/I_c$. The steady state fraction of *cis* nematogens within a domain determines the degree to which the order parameter Q of the domain has been diminished. A further important factor is the ratio of the number density of photo-active chromophores to the total number density of nematogens, which we will denote by A. The free energy density of the domain, f, is given by

$$f = f_{nem}(Q, \bar{n}_c, \underline{n}, T_0, A) + f_{el}(\underline{n}_0, \underline{n}, Q, \underline{\underline{\lambda}}, T_0, \bar{n}_c, A), \quad (17)$$

where f_{nem} is the nematic free energy, which can be taken (*31*) as a modified form of the canonical Maier–Saupe mean field free energy, while f_{el} is the elastic free energy of Equation (7). The parameter A appearing in these two expressions is the fraction of nematogens that are photo-active before any illumination. This energy is that of a monodomain misaligned from the polarisation direction by an angle θ. One must minimise over the best choice of the deformation $\underline{\underline{\lambda}}$ to get the resultant deformation just as for the monodomain aligned with $\underline{E}$ in Figure 13 where $\theta = 0$. Note that the initial director angle θ_0 has changed in general to θ – we allow director rotation if it decreases energy, a process much enhanced in elastomers over analogous liquid crystals since rotational energies are much higher. We use this energy as a starting point for polydomains, where this energy would be that for a particular domain and the deformation must be a compromise obtained by summing over all domain orientations θ, to which we now turn.

3.1 Polydomain nematic photo-elastomers

The equilibrium mechanical response of irradiated thin films of azo-containing polydomain nematic elastomers can be modelled (*31*, *34*) using the energy above. Figure 14 shows light polarised along the z direction incident on a polydomain sample containing azo chromophores; the highlighted region has current director $\underline{n}$.

The temperature T_0 appearing in the free energy densities in Equation (17) sets the initial order parameter of the individual domains. The elastic part of the free energy depends both on the original orientation of the domain $\underline{n}_0$ as well as the current orientation, while the nematic part only depends on the current orientation $\underline{n}$. The scale of the nematic contribution is set by the number density of nematogens n_n, while that of the elastic contribution is set by the number density of network crosslinks n_x, which might typically be in the ratio $n_x/n_n \sim 1/50 - 1/10$.

The total free energy density f_{tot} is then given by integrating the free energy density f over all initial domain orientations θ_0. The authors assumed a uniform deformation gradient over the whole sample. This is an approximation known as the Taylor limit. The equilibrium contraction along the direction of the optical electric field for a strongly crosslinked sample with $n_x/n_n = 1/10$ is shown in Figure 15(a), while Figure 15(b) shows the result for a weakly crosslinked sample with $n_x/n_n = 1/50$.

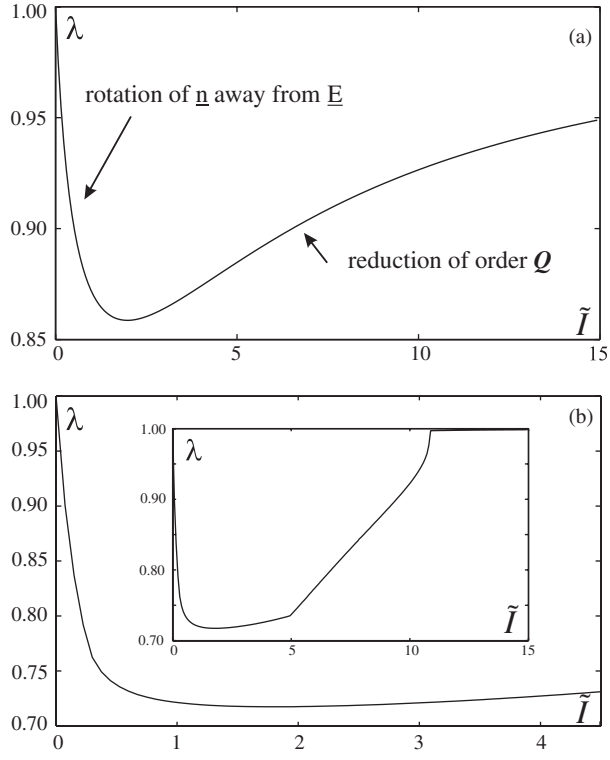

Figure 15. The equilibrium contraction, λ, along the polarisation direction of light, against reduced intensity of light, $\tilde{I}$. (a) for a strongly crosslinked elastomer with $n_x/n_n = 1/10$; (b) for a weakly crosslinked elastomer with $n_x/n_n = 1/50$.

Both samples have been taken to have an order parameter in each domain of $Q = 0.61$ before irradiation. Focussing on pane (a), the deformation gradient λ is non-monotonic with increasing intensity $\tilde{I}$. For small intensities the sample contracts quite rapidly, but as the intensity is increased the sample begins to return to its original state. At sufficiently high intensities, even those domains which are perpendicular to the polarisation direction of the incident light can absorb sufficiently to destroy their nematic order. This loss of order once again restores global isotropy and demands that the sample again be undistorted. The effects are much more pronounced in the weakly crosslinked case. Figure 15(b) shows that, by $\tilde{I} \sim 10.5$, global isotropy has been almost entirely restored and above this intensity we have $\lambda \sim 1$. The spontaneous contraction on going from a single monodomain to the isotropic state for this initial order parameter using our current freely jointed chain model would be, using Equations (3) and (11), $\lambda_m = ((1-Q)/(1+2Q))^{1/3} = 0.56$ (the form differing from before since here order is lost rather than gained). Clearly in a system of polydomains the maximal response is less – the deviation $\lambda_m - 1$ from the original state is about a third of the monodomain case: maximal polydomain response corresponds to director rotation away from the optical field for some domains contributing to contraction, but passivity for domains already at high angles to the field, and hence a compromise deformation overall.

The behaviour of the current domain order parameter Q and orientation θ of each domain as a function of the initial orientation of the domains θ_0 for several values of the reduced intensity are shown in Figures 16 and 17 for both the strong and weakly crosslinked cases.

In the strongly crosslinked case, for small intensities to the left of the stationary point in Figure 15(a), domains tend to rotate away from the electric field, which allows them to preserve more of their nematic order. Ultimately as the intensity is increased beyond the stationary point, domains tend to rotate back towards their initial orientation, and their order parameters $Q(\theta_0)$ are significantly depressed. Focussing now on the weakly crosslinked case, we see that for small intensities domains tend to rotate away from the director as for the strongly crosslinked case. However, increasing the intensity to $\tilde{I} = 0.3$, rotations away from the polarisation direction are now much larger; most domains are now nearly perpendicular to the polarisation direction. Once the intensity is increased beyond $\tilde{I} = 5$, domains that were initially aligned close to the electric field have now begun to rotate back towards the field. As the intensity continues to increase domains continue to rotate back towards their initial orientation. Ultimately by the time $\tilde{I} = 12$ all domains have returned to their initial orientation, and the sample is largely isotropic.

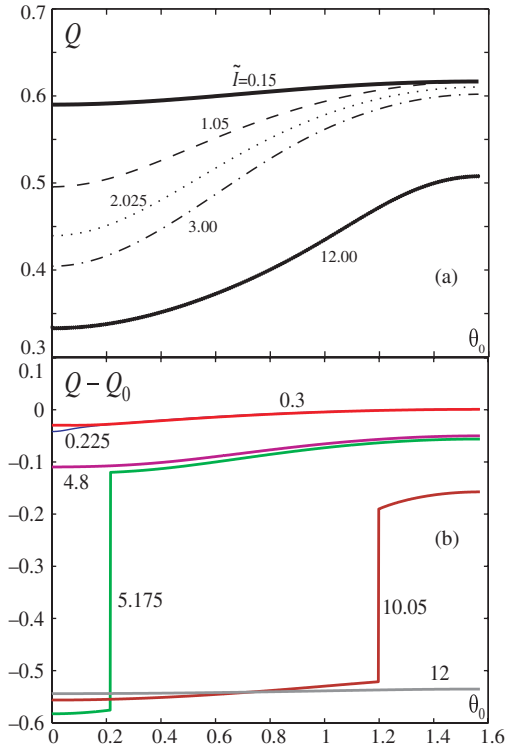

Figure 16. The order parameter Q of a domain as a function of its initial orientation θ_0 for various reduced intensities, $\tilde{I}$, taken from (*34*). Angles are measured with respect to the optical electric field. (a) A strongly crosslinked elastomer with $n_x/n_n = 1/10$. (b) A weakly crosslinked elastomer with $n_x/n_n = 1/50$, note in this case we plot $Q - Q_0$.

The non-monotonic character of contraction $\lambda < 1$ against incident intensity $\tilde{I}$ has particularly interesting consequences when one considers thicker samples where attenuation of light through the sample is significant; changing the sign of $d\lambda/d\tilde{I}$ would then allow one to reverse the direction of bending produced by attenuation – see Section 4.

3.2 *Nuclear magnetic resonance*

Nuclear magnetic resonance (NMR) spectroscopy monitors the frequency associated with transitions between nuclear spin energy levels in the presence of a fixed magnetic field. Nuclei which have a quadrupole moment produce spectral splittings which provide information about their orientation relative to the fixed field, and about the local nematic order parameter (*35*). Thus if the mesogens within an elastomer are doped with nuclei possessing a quadrupole

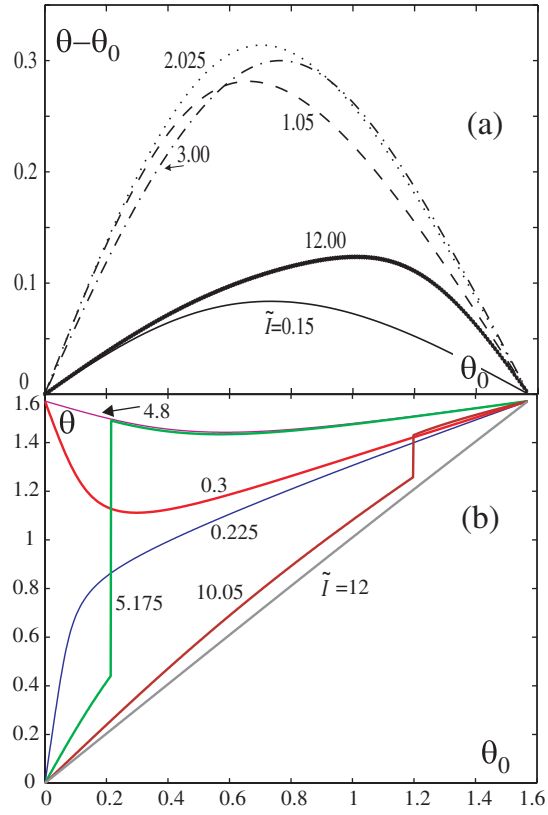

Figure 17. The director orientation θ of a domain as a function of its initial orientation θ_0 for various reduced intensities, $\tilde{I}$, taken from (*34*). Angles are measured with respect to the optical electric field. (a) A strongly crosslinked elastomer with $n_x/n_n = 1/10$, note in this case we plot $\theta - \theta_0$. (b) A weakly crosslinked elastomer with $n_x/n_n = 1/50$.

interaction we can gain information about the local ordering and orientation of the mesogens. Since elastomers have fluid-like dynamics at the microscopic scale the spectra tend to give information about the time-averaged values of the orientation and order. The simplest geometry to analyse has the fixed magnetic field of the NMR spectrometer aligned with the polarisation direction of the incident light.[1] In this geometry the NMR spectrum is given by

$$p(\omega) = \int_0^{\frac{\pi}{2}} \Big\{ [1 - \phi(\tilde{I}, Q, \theta)] \sum_{\pm} \delta(\omega \pm Q(\theta) P_2(\cos\theta)) + 2\phi(\tilde{I}, Q, \theta)\delta(\omega) \Big\} \sin\theta_0 d\theta_0, \tag{18}$$

where ω is a scaled angular frequency (it is the actual frequency relative to the Larmor frequency divided by the characteristic frequency of the quadrupole interaction) and the function ϕ is the steady state fraction of *cis* nematogens relative to the total number of nematogens, i.e. $\phi = \bar{n}_c/A$. The δ functions arise because we neglect T_2 lifetime effects – see below. The first two terms show that when quadrupole interactions are present the NMR frequency of a particular domain currently at θ is dependent upon both the local order parameter $Q(\theta)$ and directly on the orientation of the domain with respect to the magnetic field, as represented by the $P_2(\cos\theta)$ term. The final term represents the effects of the generated *cis* molecules, which are here assumed to be ordered randomly and thus only contribute at the Larmor frequency. In fact, although the *cis* molecules are bent, it is still possible that the nematic environment provided by the liquid crystal host plus the remaining *trans* molecules might induce (perhaps weaker) nematic order in the *cis* fraction. (See (*36*) for a careful investigation of the liquid crystal case.) In the event of induction of order also into *cis* molecules in an LC elastomer environment, the latter δ peak of Equation (18) would also be split. This is a subject of current research in LC azo-liquids and elastomers.

The integral over the delta functions can be performed, giving

$$p(\omega) = 2\int_0^{\frac{\pi}{2}} \phi(\tilde{I}, Q, \theta) \sin\theta_0 d\theta_0 + \sum_{\pm} \sin(f^{-1}(\pm\omega)) \frac{[1 - \phi(\tilde{I}, Q, \theta)]}{\left|\frac{df}{d\theta_0}\right|}\Bigg|_{\theta_0 = f^{-1}(\pm\omega)}, \tag{19}$$

where $f(\theta_0) = Q(\theta)P_2(\cos\theta)$. There are thus divergences in the spectrum when $\frac{df}{d\theta_0} = 0$ (provided $\sin(f^{-1}(\pm\omega)) \neq 0$). In Figure 18 we show the predicted NMR spectra for a variety of intensities for the weakly crosslinked sample discussed previously; these spectra should be viewed in conjunction with the results

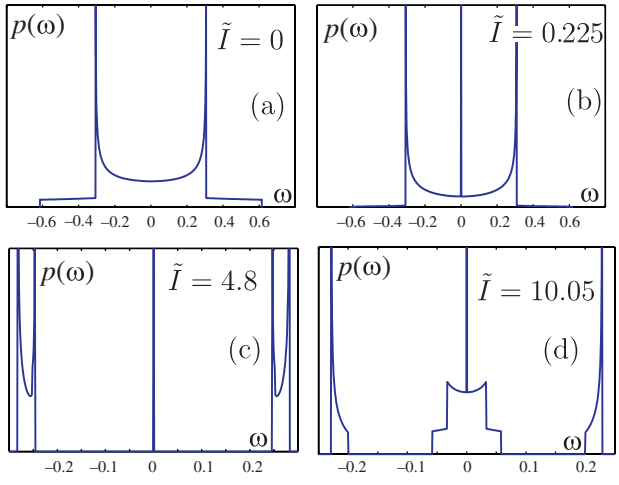

Figure 18. The predicted NMR spectra for a weakly crosslinked polydomain elastomer illuminated by linearly polarised light. The fixed magnetic field of the NMR spectrometer is parallel to the polarisation direction of the light.

for the order parameter and orientation shown in Figures 16(b) and 17(b).

Figure 18(a), which is for zero intensity, shows a spectrum with Pake lineshape typical of isotropic systems. The domains at $\theta_0 = \pi/2$ give rise to the divergences around $\omega = \pm 0.3$ while the domains at $\theta_0 = 0$ give rise to the finite discontinuities at $\omega = \pm 0.6$. Increasing the intensity to $\tilde{I} = 0.225$ (pane (b)) induces few changes; intensity appears to have moved away from the sidebands between $\omega = \pm 0.3$ and $\omega = \pm 0.6$; this happens as domains rotate away from the electric field orientation. There is also a new peak at $\omega = 0$, which corresponds to the generated *cis* molecules which do not contribute to the nematic environment. Increasing the intensity to $\tilde{I} = 4.8$ gives substantial changes in the spectrum, which has separated into a continuous region between $\omega = \pm 0.3$ and $\omega \sim \pm 0.25$ and a single peak at $\omega = 0$ from the *cis* molecules. The separation of the peaks corresponds to all domains, independent of their initial orientation, now being almost perpendicular to the field. Increasing the intensity drastically to $\tilde{I} = 10.05$, pane (d), we again see isolated peaks between $\omega = \pm 0.25$ and $\omega = \pm 0.2$ which correspond to domains currently close to $\theta \sim \pi/2$. We also see the presence of a Pake spectrum between $\omega \sim -0.05$ and $\omega \sim 0.05$ which corresponds to domains which are aligned roughly with their initial orientation, i.e. $\theta \sim \theta_0$, but which have a significantly smaller nematic order parameter as a result of illumination. Also present is the usual peak at $\omega = 0$ generated by the *cis* molecules. Increasing the intensity still further results in the growth of the central Pake spectrum at the expense of the sidebands as domains continue to return to their initial orientation.

In practice there is line-broadening because of T_2 lifetime effects. A decay like $e^{-t/\tau}$ corresponds rather to convolution not with a δ function in Equation (18), but with a Lorentzian. Thus the features in the ideal NMR spectra will be rounded, to an extent determined by the underlying quadrupole splitting ($\delta\omega$) relative to the intrinsic (Lorentzian) line broadening of extent $1/\tau$. Typical numbers for nematic elastomers are $\delta\omega \sim 3 \times 10^5$ rad s^{-1} and $\tau \sim 150\,\mu$s, showing that resolution of spectral structure should be easily possible.

4. Non-uniform response

For thicker elastomer films, the attenuation of light caused by the *trans* $\rightarrow$ *cis* isomerisation becomes important. Illumination and the subsequent changes in the order parameter change the natural length of the sample, a gradient in illumination then creates a gradient in natural length and the cantilever responds by bending. Warner and Mahadevan (*37*) investigated

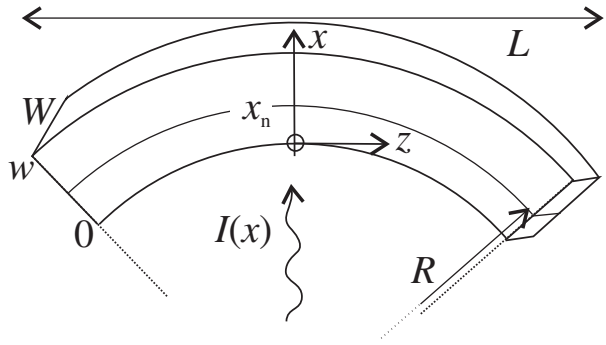

Figure 19. A photo-cantilever, with the director along the z-axis, illuminated with light travelling along the x-axis; adapted from (*37*).

the mechanical response of illuminated films of photo-active elastomers in the limit of small strain elasticity. They analysed the situation shown in Figure 19 where the director $\underline{n}$ is aligned along the z-axis, and the illuminating light travels along the x-axis.

The effect of illumination and thus of the subsequent changes in the order parameter are modelled by a change in the natural length of the sample along the z-axis. This is a photo-strain ϵ_{zz}^{photo}. Mostly it is a contraction along the director and hence $\epsilon_{zz}^{photo} < 0$. The simplest assumption is that it is proportional to the intensity $I(x)$ of light at this depth x. Thus we take the photo-strain relative to the new natural length to be $-cI(x)$, with c a constant. We assume this in our first case, that of linear absorption, but more complicated connections between irradiation and natural length change probably exist when there are very large changes of nematic order, to which we return in the non-linear case. The total strain relative to the local zero stress state is thus given by $\epsilon_{zz} = \frac{x}{R} + K - cI(x)$ where R is the radius of curvature adopted by the cantilever, and K is the mean contraction/expansion of the sample. For the cantilever shown with $w \lesssim W \ll L$, the only non-zero component of the stress tensor is the zz component, which is given by

$$\sigma_{zz} = Y\left[\frac{x}{R} + K - cI(x)\right], \tag{20}$$

where Y is the Young's modulus for strain along the director; in principle Y can vary with depth x because of compositional gradients (*38*), gradients of liquid crystalline order (*18*) or photo-induced changes in structure, that is, $Y(I(x))$. The radius and mean contraction are determined by demanding that the total force in the z direction across any cross section is zero, and similarly for the torque about the y direction (since the bending is spontaneous, that is without external torques being applied):

$$f_z = 0 = \int_{x=0}^{x=w} Y\left[\frac{x}{R} + K - cI(x)\right]dx,$$
$$M_y = 0 = \int_{x=0}^{x=w} Yx\left[\frac{x}{R} + K - cI(x)\right]dx. \quad (21)$$

These mechanical equilibrium conditions are of course applicable to any solids, not just elastomers but also glassy nematic photo-cantilevers – see for example (*38*) for this method applied to such materials. One requires simply the connection between photo-strain and intensity.

In this simple treatment we have ignored curvature of the opposite sign in the *xy* plane arising from Poisson ratio (volume conservation) effects – *zz* contraction below the neutral surface causes *yy* elongation, with the reverse above the neutral surface. The resulting curvature at right angles to the original curvature creates a saddle, that is, an anticlastic surface. However, for *xz* curvature great enough, the *xy* curvature makes the *xy* section deviate too greatly from the neutral surface, greatly accentuating the *zz* stretches and compressions at great energy cost. The transverse curvature is then suppressed and anticlasticity can be ignored, except in small boundary regions near the cantilever edges (*39*).

The study (*37*) focussed on photo-effects; however, the basic prescription of external fields causing a change in the natural length and a resulting mechanical response is quite general and is essentially identical to the analysis of the bending of bimetal strips upon a change in temperature provided by Timoshenko (*40*) and indeed the bending of a nematic elastomer in response to a temperature gradient has been analysed using this method by Hon *et al.* (*41*). We now proceed to examine two different types of profile $I(x)$, and another possible relation between photo-strain and I.

4.1 Linear absorption leading to mechanical response

It remains to specify $I(x)$, the profile of intensity, and thus, in this model, the profile of *zz* photo contraction to a new relaxed state. The simplest variation of intensity is attenuation (photons absorbed) by dye at a rate proportional to the intensity itself, $dI/dx = -I/d$, which is the classical Lambert–Beer law of linear absorption, that is, $I(x) = I_0 e^{-x/d}$, where d is the Beer absorption length, which is proportional to the inverse of the absorption cross section Γ of (15), and I_0 is the incident intensity. With this exponentially decaying intensity $I(x)$, one can evaluate (*37*) relations (21) analytically and then solve them for the reduced curvature $(wcI_0)/R$ as a function of the Beer length reduced by the cantilever thickness d/w; see Figure 20.

Note that for non spatially-varying Y the modulus cancels out of the equilibrium equations. The photo-strain $-cI_0 e^{-x/d}$ prefactor is its (maximal) value at the upper surface, $-cI_0$. It can be taken out of the integral whereupon curvature then scales with cI_0. The curvature is non-monotonic: very little penetration ($d/w \ll 1$, thick cantilevers) sees only a contraction of a thin skin which is resisted by the bulk material and curvature vanishes. In the thin limit $d/w \gg 1$, contraction is nearly constant (appearing as K), and not differential, on going through the cantilever, and again little curvature results. Maximal curvature for linear absorption occurs at $d/w \sim 0.3$.

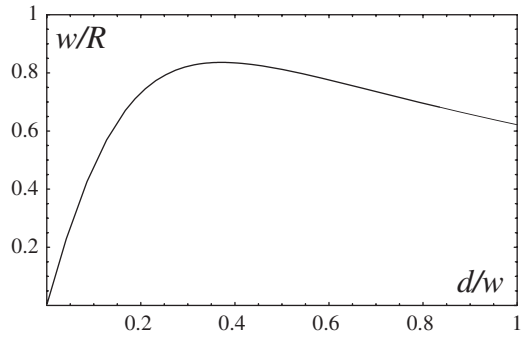

Figure 20. Reduced curvature w/R against Beer absorption length reduced by the cantilever thickness, d/w.

It is necessary that, in order for the force and torque to vanish, there are two neutral surfaces where the stress vanishes, rather than one such surface as in a cantilever bending in response to external loading. Such surfaces are at depths x_n where the geometric strains arising from curvature match the local photo-strain, that is, $x_n/R + K + cI(x_n) = 0$. Non-linear absorption will turn out to lead to sometimes three or more neutral surfaces; see (*37*, *42*) for more details.

4.2 Non-linear absorption and mechanical response to intense beams

The appropriate form for the decaying intensity $I(x)$ to inject into Equation (21) for bending is particularly important. The treatment above assumed the exponential Lambert–Beer law. However, when one considers the detailed chemistry of the samples of Yu (*19*) it becomes apparent that the azo doping is so high that Beer's law would dictate that the vast majority of the light would be absorbed within a very thin surface layer of about 60 nm, which is much thinner than the cantilever ($\gtrsim 50\,\mu$m) that they employed. It is then difficult to see how much of a bend can be induced at all, since the vast bulk of the sample is apparently un-irradiated and hence resists bending; the $d/w \to 0$ limit of Figure 20. We argue that light beams must be sufficiently intense to give non-linear absorption and hence deep penetration.

Assuming that the background network is transparent to the incident light, and that the incident light

does not activate the *cis* → *trans* back isomerisation, the attenuation of light is described by

$$\partial I/\partial x = -In_t/d, \tag{22}$$

where $I = I(x,t)$ is the intensity at depth x within the film and time t. If n_t were a constant this equation would integrate to give the standard Lambert–Beer law for attenuation $I(x) = I_0 \exp(-xn_t/d)$. Thus the approximation of weak beams is simply that there is no appreciable photo-induced change of the *trans* fraction of dye molecules. Thus another implication of a truly linear absorption is that there is no dynamics associated with the process – n_t is constant and therefore so is the profile $I(x)$.

However the fraction of *trans* molecules may not be constant. As shown in Equation (15), the dynamics of the *trans* fraction depends on the intensity, and thus the *trans* fraction will vary with position as well as time. Solving for the intensity and the *trans* fraction involves solving a pair of coupled first order partial differential equations. A largely analytical solution of these equations is provided by Corbett *et al.* (*43*) and investigated experimentally by Serra *et al.* (*44*).

We first focus on the steady state intensity (*42*) through the cantilever. Setting $\partial n/\partial t = 0$ in (15) and solving for n_t gives

$$n_t(x) = \frac{1}{1+\tau\Gamma I(x)} = \frac{1}{1+\alpha I(x)/I_0}, \tag{23}$$

where $\alpha = \Gamma\tau I_0 \equiv I_0/I_c$ and I_0 is the intensity of the incident light. For simplicity, we take a constant Q (absorbed into Γ) and set $\theta = 0$; light is polarised along the (unchanging) director. Inserting this form into Equation (22) and integrating gives

$$\ln\left(\frac{I(x)}{I_0}\right) + \alpha\left(\frac{I(x)}{I_0} - 1\right) = -\frac{x}{d}. \tag{24}$$

Solutions for the reduced intensity are $I(x)/I_0 = \frac{1}{\alpha} W_L(\alpha e^{\alpha-(z/d)})$ in terms of the standard Lambert-W function $W_L(x)$ (the ProductLog function of Mathematica) and are shown for several values of α in Figure 21.

Values of α can range from $\alpha \sim 0$ in the Beer limit, to several hundreds in the limit of intense beams. We see from (24) that for large $\alpha \gg 1$ the intensity is approximately $\frac{I(x)}{I_0} = 1 - x/(\alpha d)$, a linear form which implies that the light penetrates the cantilever significantly further than would be expected based on the Lambert–Beer exponential law. At $t = 0$ we have a Lambert–Beer law, since initially $n_t(x, t = 0) = 1$ and spatially integrating (22) is trivial. As time progresses, the *trans* molecules near the surface are converted to *cis* molecules which allows the light to penetrate further into the sample.

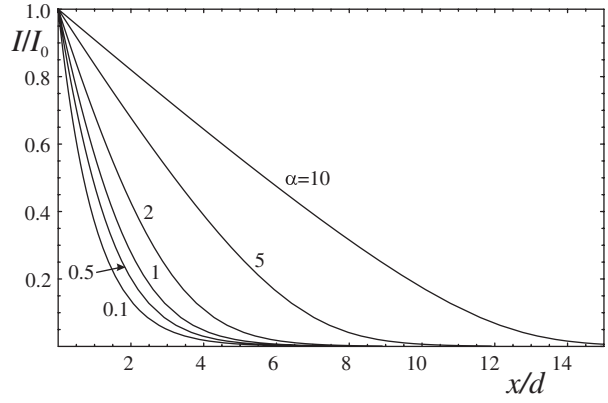

Figure 21. Intensity normalised by its incident value as a function of x/d for various values of α, taken from (*42*).

There is a propagating front of bleaching which we discuss in the next section, Section 4.3 on dynamics. The steady state of intensely irradiated azo dyes in solution has been investigated experimentally by Statman and Janossy (*45*) in agreement with the intensity profile above. Note that we have continued to ignore here the optically induced back reaction of *cis* to *trans*; see (*42*, *46*) for more details of these and other effects.

In the non-linear case there is an appreciable bleaching of the *trans* population (this is what allows the deeper penetration of the light) and hence an appreciable growth of the *cis* population. It is the latter that disrupts the nematic order and thus leads to strain. With perhaps more accuracy, in (21) we instead take the photo-strain to be proportional to $n_c(x)$, with a constant of proportionality that we absorb into $1/R$ and into K for simplicity. The *cis* population derives from (23):

$$n_c(x) = \frac{\alpha I(x)/I_0}{1+\alpha I(x)/I_0};$$

see Figure 22 for $n_c(x)$ at various incident beam intensities α.

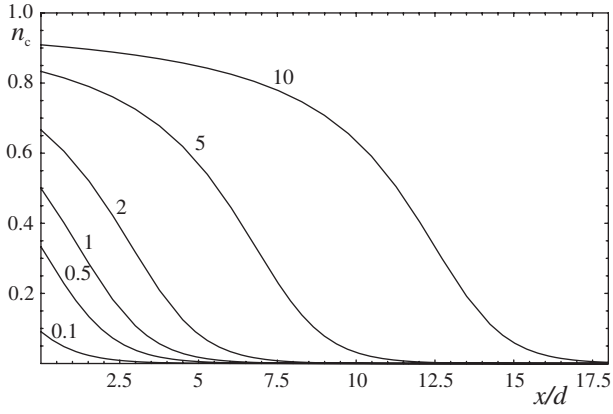

Figure 22. *cis* fraction $n_c(x)$ as a function of reduced x/d for various values of α, taken from (*42*).

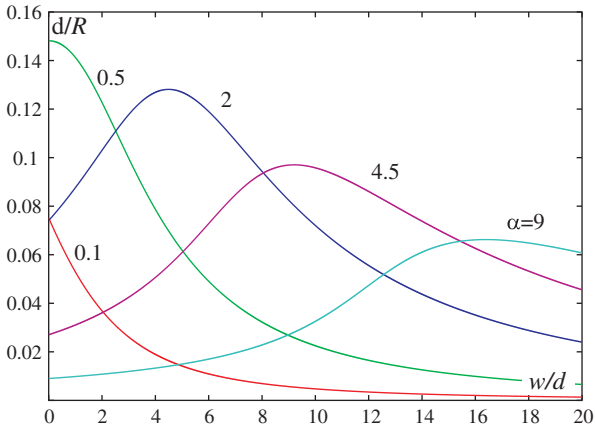

Figure 23. Reduced curvature d/R as a function of reduced cantilever thickness w/d for various values of α, taken from (*42*).

Weak beams create few *cis* molecules and they are only at the upper surface. Strong beams create a high *cis* fraction and thereby penetrate deeper. A developed profile of *cis* will create a varying photo-strain and thus curvature as one sees in Figure 23 for curvature as a function of cantilever thickness.

With this scaling of curvature (by $1/d$), weak ($\alpha < 0.5$) optical beams induce less curvature as cantilevers become thicker. For more intense beams, there is instead an optimum thickness to produce curvature. Note that intense beams can cause cantilevers, thicker by many times the linear absorption length d, still to bend, even though Beer analysis would suggest light would not have significantly penetrated the cantilever. This is presumably the basis of the light-induced bend of very heavily dye-loaded photo solids. Non-linear absorption is undoubtedly very important in practical situations.

Examples of extreme bend of nematic network solids include an elastomer from Palffy-Muhoray *et al.* (Figure 24) and a glassy nematic polymer from White *et al.* (*47*) (Figure 25).

More subtle forms of bend can also be achieved by a director distribution through the cantilever that is non-uniform, for instance a splay-bend distribution in going from planar alignment at one surface to homeotropic

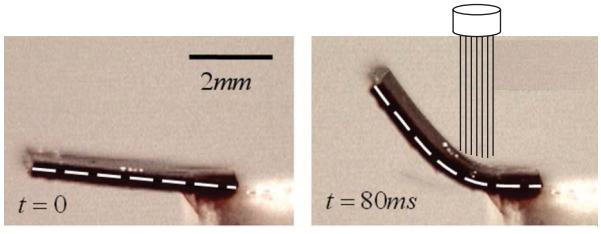

Figure 24. A nematic elastomer cantilever with dye being illuminated by a green laser. Bend is very fast and drastic. It is possible that some heating effects are also active.

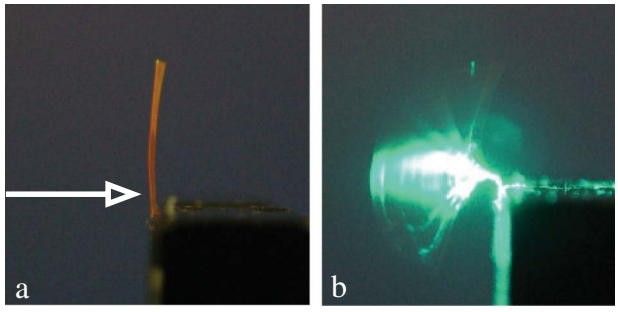

Figure 25. An azo-benzene nematic cantilever (a) before illumination – the white arrow shows the direction of the beam from side (b) intensely illuminated from by beam. The cantilever bends across the light beam and is thus induced to bend back again, thereby oscillating. The oscillations were at about 25 Hz, the precise value being seemingly determined by where the beam struck and therefore the inertia of the upper moving part. Higher beams led to higher frequencies.

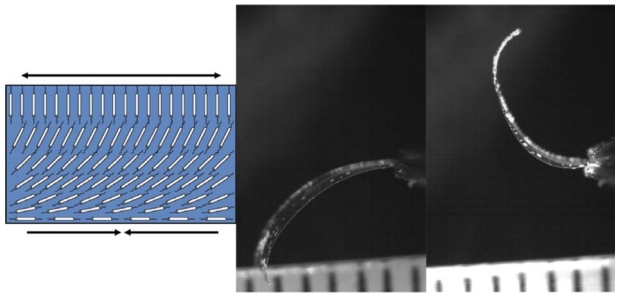

Figure 26. A nematic network photo-cantilever (left) with a splay-bend director distribution through its section. The cantilever (middle figure) bends upwards (right) on illumination.

on the other. Such delicate photo-cantilevers have been made by van Oosten *et al.* (*48*); see Figure 26.

Mechanical contractions (along the director) and elongations (perpendicular to the director) that cause bend on illumination are indicated on the schematic of the director distribution through the cantilever's section. Clearly, attenuation of the optical beam is not necessary, nor does it matter from which side the cantilever is illuminated! The equilibrium equations (21) now have both a modulus and also a photo-strain that vary with position because the director is rotating. The equations are more complex, but the principles are the same. When there is instead an internal twist director distribution, beautiful spiral rather than simply curved structures result from illumination of the cantilever (*18*); see Figure 27.

4.3 The dynamics of non-linear absorption and cantilever bend

As a *cis* population is created, the medium becomes more transparent to the incident light and it penetrates

Figure 27. A nematic network photo-cantilever with a twist director distribution through its section curls (right) on illumination (*18*).

more deeply. This process is not instant since sufficient optical energy has to be delivered in order to convert the *trans* dye molecules. In its simplest form with $\underline{\mathrm{E}}$ along $\underline{n}$ and ignoring Q changes, the population dynamical equation (15) reduces to the first of

$$\begin{aligned} &\partial n_t(x,t)/\partial t = \frac{1}{\tau}\left((1+\alpha\frac{I(x,t)}{I_0}n_t)+1\right), \\ &\partial I(x,t)/\partial x = -In_t/d. \end{aligned} \tag{25}$$

The second, Beer-like equation for the spatial decay clearly involves an absorbing species population that is a function of both time and space. From the former equation, we see that times will scale with τ. To solve this pair of non-linear, coupled, partial differential equations exactly (*43*), use the absorption $A(x,t) = -\ln(I/I_0)$ as the variable. $\mathcal{A}$ is most useful in the linear case since as a log it compresses an exponential range of intensities, but it has useful aspects in the non-linear case too: it reflects the absorber number in the optical path. Rearranging the second of Equation (25) to

$$\frac{1}{I}\frac{\partial I}{\partial x} = -n_t(x,t)/d$$

and integrating the sides as $\int_1^{I/I_0} d(I/I_0)$ and $\int_0^x dx$, one obtains for all times and incident intensities (recall that $I(0,t)/I_0 = 1$ for all t)

$$A(x,t) = \frac{x}{d}\bar{n}_t \equiv \frac{x}{d}\frac{1}{x}\int_0^x dx' n_t(x',t), \tag{26}$$

where $\bar{n}_t$ is the mean *trans* number fraction through the sample. However, in the non-linear limit the average $\bar{n}_t$ is no longer independent of x. Thus the quantity $\bar{n}_t/d = \mathcal{A}(x,t)/x$ is no longer a simple, material-dependent extinction coefficient but depends on depth in the sample.

Denote partial spatial and temporal derivatives of X by X' and $\dot{X}$, respectively. Differentiating Equation (26) with respect to t and using the first of (25) for $\dot{n}_t$ under the integral yields

$$\mathcal{A} = \int_0^x dx'[1-(1+\alpha I/I_0)n_t]/(\tau d).$$

Now use $n_t/d = \mathcal{A}' = -I'/I$ with the boundary condition $\mathcal{A}(0,t) = 0$ to obtain

$$\begin{aligned} \tau\dot{\mathcal{A}} &= x/d - \int_0^x dx(1+\alpha\mathcal{I})\mathcal{A}' \\ &= \frac{x}{d} - \mathcal{A} + \alpha(I/I_0 - 1) \equiv \frac{x}{d} - \mathcal{A} \\ &\quad + \alpha\left(\mathrm{e}^{-\mathcal{A}} - 1\right). \end{aligned} \tag{27}$$

A final quadrature gives $\mathcal{A}(x,t)$:

$$t/\tau = \int_{x/d}^{\mathcal{A}} \frac{d\mathcal{A}}{x/d - \alpha - \mathcal{A} + \alpha\mathrm{e}^{-\mathcal{A}}}. \tag{28}$$

The initial absorption $\mathcal{A}(x, t=0) = x/d$, Beer's law, at $t = 0$ is obtained from the vanishing of each side of Equation (28). The vanishing of the right-hand side demands that the limits of the integral tend to each other. The long time limit $t/\tau \to \infty$ is achieved when the integrand's denominator vanishes, from which one obtains Equation (24), and thus the ProductLog solution.

One can illustrate the profile dynamics by varying thickness and incident power. Figure 28 shows $\mathcal{I}(x,t)$ $(\equiv \mathrm{e}^{-\mathcal{A}(x,t)})$ for reduced intensity $\alpha = I_0/I_c = 10$ against x for a set of times t.

Initially at $t = 0$, the profile $I(x,0)/I_0$ is exponential, and at long times ($t = 5\tau$) the profile is essentially linear out to $x \sim \alpha d = 30d$; then it decays exponentially, as the other curves eventually do, at still greater depth. At intermediate times the profile first saturates (bleaches) at small x, that is, it approaches the initial part of the equilibrium profile. Then, as the surface layers let more light through, the profile deeper down

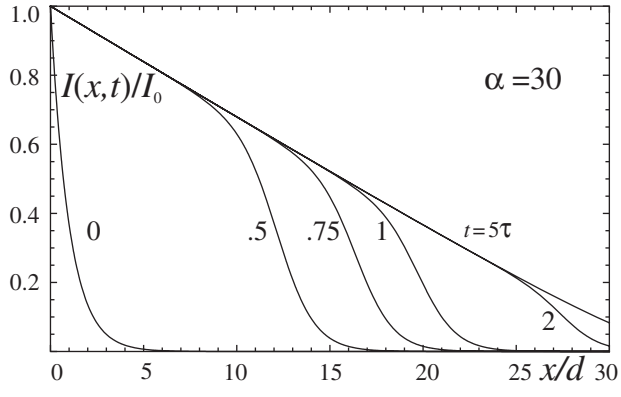

Figure 28. Intensity against reduced depth x/d for reduced incident intensity $\alpha = 30$ (reduced times marked).

also approaches the non-Beer form. A front of bleaching (sharper at greater α) propagates through the sample. See (*43*) for the comparison of fronts with different α. The intensity of any emergent light is far in excess of any Beer expectation. Its rate of build up is interesting. However, the intensity profile in Figure 28 is not in general directly observable, although it is clearly the determinant of mechanical bending. Experimentally one explores bleaching by measuring the dynamics of the build-up of reduced intensity of the light emerging at the back face $x = w$ of a sample, i.e. the transmission $I(w,t)/I_0$. See (*43*) for theoretical analysis and graphs, and (*38*, *44*) for experimental non-linear dynamical results for the emergence of bleaching fronts at the back sample face. Intensity only builds up in time from the Beer result at $t = 0$ because of dye population changes and Figure 29, adapted from (*44*), shows the arrival of bleaching fronts and thus demonstrates departure from Beer's law.

As light penetrates more deeply and converts more dye to its order-reducing *cis* form, so the photo-strain builds up and then also so does photo-bend. One can predict the dynamics of bending with the simple assumption that it is limited by the conversion of *trans* to *cis*, that is, the build up of photo-strain rather than by the dynamical response of the network *per se*. One uses $I(x,t)$ from above to determine $n_c(x,t)$ and thus the time and space-dependent photo-strain that has to enter the mechanical equations (21). The result is a scaled curvature $d/R(t,\alpha)$, the incident intensity no longer appearing as a simple scaling in the non-linear case. An example of such bending dynamics, theory and experiment is given in (*38*); see Figure 30.

The bending is initially very slight since the profile is Beer-like and penetration rather small at these dye loadings. In time the penetration and thus bend

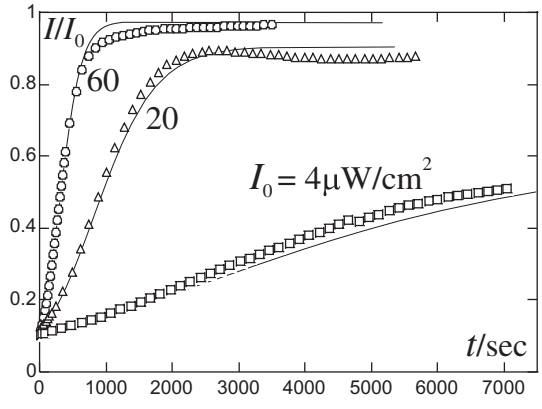

Figure 29. Reduced emergent intensity, $I(w, t)/I_0$, at the sample's back face $x = w$ against time, t, for various incident intensities, I_0 (*44*). Solid lines are fits to theory for $w/d = 2.2$.

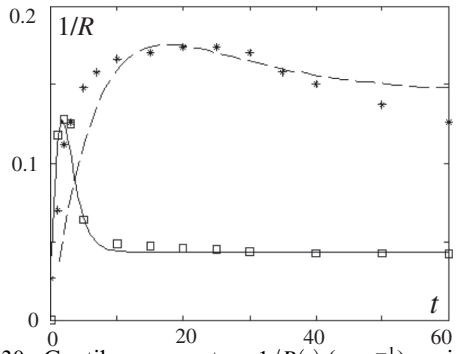

Figure 30. Cantilever curvature $1/R(t)$ (mm^{-1}) against time (s) for reduced incident intensity $\alpha = 6$ for dye loadings of 1.4% (squares) and 4% (*). Lines represent theory, with fitted relaxation rates τ. See (*38*).

increases, but then decreases as the penetration gives a weaker variation of photo-strain with depth. One can even reverse the sense of bending of a cantilever as irradiation proceeds. Curvature reversal was suggested as a consequence of non-monotonic response of polydomain nematics, Figure 15 and discussion. Another method is to have a spatially dependent modulus $Y(x)$ through the cantilever thickness. Equilibrium conditions (21) make clear that as a bleaching front penetrates regions with different Y, they can prevail and alter the sign of curvature; see (*38*) for experiment and theory. In a third method one can pre-treat both surfaces of a cantilever with UV to create *cis* -rich contractile surfaces. If one side is then irradiated with light of another colour that induces a *cis* – *trans* shift, then the mechanical imbalance between the surfaces causes bend; see (*49*).

5. Summary and outlook

We have seen how concepts envisaged by de Gennes many years ago, concerning the coupling of nematic order to mechanics once one has a nematic solid, have been developed theoretically and experimentally to yield new and complex phenomena.

There remain many questions for the future. We have given two connections between photo-strain and optical intensity. However, the effects of order parameter change and director rotation in this connection are still to be fully incorporated into cantilever bending in the way they were for polydomain response. The feedback between compression (in regions of the cantilever) and director rotation have likewise not been considered.

Glassy systems are interesting because they have larger moduli, which may be important in some applications. There is currently no available theory at the level developed for the de Gennes elastomeric systems. The situation is very open, not just on the mechanical

and liquid crystal ordering side, but also because glassy environments clearly have an influence on non-linear absorption dynamics.

The future for photo-responsive nematic solids now probably rests in applications since they will give focus to further theoretical and fundamental experimental investigations. Their three-dimensional mechanics is complex. Searches are underway to find applications in microfluidic pumps, valves and mixers. Studies include shell mechanics and writable surface topographies (*37*, *50*, *51*).

Acknowledgements

We thank E.M. Terentjev, P. Palffy-Muhoray, D. Broer, T.J. White and T. Ikeda for permission to reproduce figures, and B. Zalar for a critical reading of the review and for suggestions about NMR. This work was supported by EPSRC, UK.

Note

1. Experimentally, it could perhaps be simpler to have the fixed field direction coincident with the propagation direction of the light.

References

(1) de Gennes, P.G. *Phys. Lett.* **1969**, *A28*, 725–726.
(2) de Gennes, P.G. *C. R. Acad. Sci. B* **1975**, *281*, 101–103.
(3) Tajbakhsh, A.R.; Terentjev, E.M. *Eur. Phys. J. E* **2001**, *6*, 181–188.
(4) de Gennes, P.G. In *Polymer Liquid Crystals*; Ciferri, A., Krigbaum, W.R., Meyer, R.B. Eds.; Academic Press: New York, 1982.
(5) Warner, M.; Terentjev, E.M. *Liquid Crystal Elastomers*, Revised paperback edition; Oxford University Press: Oxford, 2007.
(6) Bladon, P.; Terentjev, E.M.; Warner, M. *Phys. Rev. E* **1993**, *47*, R3838–R3840.
(7) Warner, M.; Terentjev, E.M. *Macromol. Symp.* **2003**, *200*, 81–92.
(8) Abramchuk, S.; Khokhlov, A. *Doklady Akad. Nauk SSSR (Doklady Phys. Chem.)* **1987**, *297*, 385–388.
(9) Warner, M.; Gelling, K.; Vilgis, T. *J. Chem. Phys.* **1988**, *88*, 4008–4013.
(10) Küpfer, J.; Finkelmann, H. *Macromol. Chem. Rapid. Comm.* **1991**, *12*, 717–726.
(11) Olmsted, P.D. *J. Phys. II* **1994**, *4*, 2215–2230.
(12) Kundler, I.; Finkelmann, H. *Macromol. Chem. Phys.* **1998**, *199*, 677–686.
(13) Finkelmann, H.; Kundler, I.; Terentjev, E.M.; Warner, M. *J. Phys. II* **1997**, *7*, 1059–1069.
(14) Küpfer, J.; Finkelmann, H. *Macromol. Chem. Phys.* **1994**, *195*, 1353–1367.
(15) Brand, H.; Pleiner, H.; Martinoty, P. *Soft Matter* **2006**, *2*, 182–189.
(16) Biggins, J.S.; Terentjev, E.M.; Warner, M. *Phys. Rev.* **2008**, *E78*, 041704.
(17) Mol, G.N.; Harris, K.D.; Bastiaansen, C.W.M.; Broer, D.J. *Adv. Funct. Mat.* **2005**, *15*, 1155–1159.
(18) Harris, K.D.; Cuypers, R.; Scheibe, P.; van Oosten, C.L.; Bastiaansen, C.W.M.; Lubb, J.; Broer, D.J. *J. Mat. Chem.* **2005**, *15*, 5043–5048.
(19) Yu, Y.; Nakano, M.; Ikeda, T. *Nature* **2003**, *425*, 145.
(20) Tabiryan, N.; Serak, S.; Dai, X.M.; Bunning, T. *Optics Express* **2005**, *13*, 7442–7448.
(21) Stolbova, O. *Sov. Phys. Dokl.* **1963**, *8*, 275.
(22) Stolbova, O. *Dokhl. Akad. Nauk SSSR* **1963**, *149*, 84.
(23) Eisenbach, C.D. *Makromol. Chem.* **1978**, *179*, 2489–2506.
(24) Eisenbach, C.D. *Polym. Bull.* **1979**, *1*, 417.
(25) Eisenbach, C.D. *Makromol. Chem. Rapid Commun.* **1980**, *1*, 287–292.
(26) Eisenbach, C.D. *Polymer* **1980**, *21*, 1175–1179.
(27) Finkelmann, H.; Nishikawa, E.; Pereira, G.G.; Warner, M. *Phys. Rev. Lett* **2001**, *87*, 015501.
(28) Li, M.H.; Keller, P.; Li, B.; Wang, X.G.; Brunet, M. *Adv. Mat.* **2003**, *15*, 569–572.
(29) Cviklinski, J.; Tajbakhsh, A.; Terentjev, E. *Eur. Phys. J. E* **2002**, *9*, 427–434.
(30) Harvey, C.L.M.; Terentjev, E.M. *Eur. Phys. J. E* **2007**, *23*, 185–189.
(31) Corbett, D.; Warner, M. *Phys. Rev. Lett* **2006**, *96*, 237802.
(32) Ikeda, T.; Nakano, M.; Yu, Y.; Tsutsumi, O.; Kanazawa, A. *Adv. Matter*. **2003**, *15*, 201–205.
(33) White, T.J.; Serak, S.V.; Tabiryan, N.V.; Vaia, R.A.; Bunning, T.J. *J. Mat. Chem.* **2009**, *19*, 1080–1085.
(34) Corbett, D.; Warner, M. *Phys. Rev. E* **2008**, *78*, 061701.
(35) de Gennes, P.G.; Prost, J. *The Physics of Liquid Crystals*, 2nd edn; Oxford University Press: Oxford, 1993.
(36) Zalar, B.; Lavrentovitch, O.D.; Zheng, H.; Finotello, D. *Phys. Rev. E* **2000**, 62, 2252–2262.
(37) Warner, M.; Mahadevan, L. *Phys. Rev. Lett.* **2004**, *92*, 134302.
(38) van Oosten, C.L.; Corbett, D.; Davies, D.; Warner, M.; Bastiaansen, C.W.M.; Broer, D.J. *Macromolecules* **2008**, *41*, 8592–8596.
(39) Shield, R. *Q. J. Mech appl. Math.* **1992**, *45*, 567–573.
(40) Timoshenko, S. *J. Opt. Soc. Amer.* **1925**, *11*, 233–255.
(41) Hon, K.K.; Corbett, D.; Terentjev, E.M. *Eur. Phys. J. E* **2008**, *25*, 83–89.
(42) Corbett, D.; Warner, M. *Phys. Rev. Lett* **2007**, *99*, 174302.
(43) Corbett, D.; van Oosten, C.L.; Warner, M. *Phys. Rev. A* **2008**, *78*, 013823.
(44) Serra, F.; Terentjev, E.M. *J. Chem. Phys.* **2008**, *128*, 224510.
(45) Statman, D.; Janossy, I. *J. Chem. Phys.* **2003**, *118*, 3222–3232.
(46) Corbett, D.; Warner, M. *Phys. Rev. E* **2008**, *77*, 051710.
(47) White, T.J.; Tabiryan, N.V.; Serak, S.V.; Hrozhyk, U.A.; Tondiglia, V.P.; Koerner, H.; Vaiaa, R.A.; Bunning, T.J. *Soft Matter* **2008**, *4*, 1796–1798.
(48) van Oosten, C.L.; Harris, K.D.; Bastiaansen, C.W.M.; Broer, D.J. *Eur. Phys. J. E* **2007**, *23*, 329–336.
(49) Hrozhyk, U.; Serak, S.V.; Tabiryan, N.V.; White, T.J.; Bunning, T.J. *Optics Express* **2009**, *17*, 716–722.
(50) Sousa, M.E.; Broer, D.J.; Bastiaansen, C.W.M.; Freund, L.B.; Crawford, G.P. *Adv. Mat.* **2006**, *18*, 1842–1845.
(51) Elias, A.L.; Harris, K.D.; Bastiaansen, C.W.M.; Broer, D.J.; Brett, M.J. *J. Mater. Chem.* **2006**, *16*, 2903–2912.